THE JOURNAL OF PHYSICAL CHEMISTRY A

Article

pubs.acs.org/JPCA

Pinned Chemical Waves in the Presence of Stokes Flow

Hua Ke,[†] Zhihui Zhang,[†,‡] and Oliver Steinbock*[,†,‡]

[†]Department of Chemistry and Biochemistry, Florida State University, Tallahassee, Florida 32306-4390, United States

[‡]Institute of Molecular Biophysics, Florida State University, Tallahassee, Florida 32306-4380, United States

Supporting Information

ABSTRACT: Excitable reaction−diffusion systems form a wealth of dissipative concentration patterns that exist not only in chemical systems but also control or disrupt biological functions. An important example are rotating spiral waves in the autocatalytic Belousov−Zhabotinsky reaction. We show that the viscosity of this system can be increased by the addition of the polymer xanthan gum. In the resulting system, we pin spiral waves to a thin glass rod and then reposition the vortex centers by a linear motion of the heterogeneity. The Stokes flow generated by this motion can be a weak perturbation to the wave pattern and follows a simple, analytical expression. Numerical simulations of a corresponding reaction−diffusion-flow model reproduce the experimental observations and show that the spatial extent of the flow field can vary widely around the characteristic wavelength of the spiral. We find that a sharp spatial decay of the flow pattern corresponds to our experimental observations, whereas more expansive flow fields surprisingly allow the repositioning of spiral tips at speeds faster than the wave velocity.

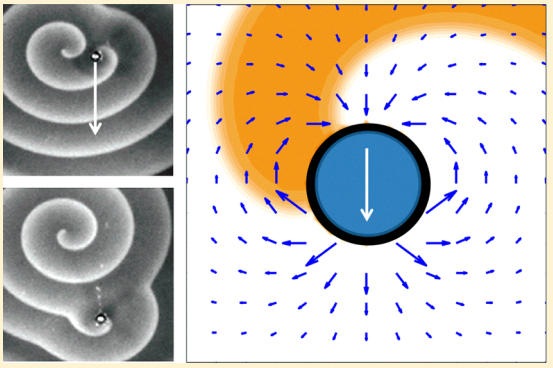

INTRODUCTION

Reaction conditions far from the thermodynamic equilibrium can induce a wealth of concentration patterns including stationary Turing patterns and traveling chemical waves.[1−3] Many of these self-organized structures enable, affect, or disrupt biological processes such the aggregation of cellular slime molds,[4] the pump action of the human heart,[5] and the uterine contractions during child birth.[6] Their fundamental dynamics are typically the result of an either excitable or oscillatory, local behavior that extends spatially by diffusion or diffusion-like mechanisms. Accordingly, chemical waves are found in many nonlinear reaction−diffusion models and have been observed in catalytic surface reactions,[7] on passivated metals,[8] and in the Belousov−Zhabotinsky (BZ), the chlorite−iodide−malonic acid, and other liquid phase reactions.[9,10]

All of the latter examples are also known to self-organize rotating excitation vortices. These concentration patterns trace Archimedean spirals and consist of periodic wave trains that emanate from the spiral tip in the center of the wave field.[11] The tip is a phase singularity and rotates on system-specific trajectories such as circles and epicycles.[12,13] Typically, these trajectories span over distances smaller than the spiral pitch. For topological reasons, spiral waves are created or destroyed as counter-rotating pairs. Their dynamics and external control have attracted considerable attention and have established an overall good understanding of these striking patterns as well as their three-dimensional counterparts.[14] For instance, it was shown that the spiral tip drift can occur in response to symmetry breaking perturbations such as periodic parameter variation,[15] static parameter gradients,[16] nearby boundaries,[13] and spiral interaction.[17]

Most studies of spiral waves in chemical systems use the autocatalytic BZ reaction, which involves the oxidation of malonic acid by bromate in an acidic medium.[1] The reaction is catalyzed by redox couples such as ferroin/ferriin, Ce(III)/Ce(IV), and Ru(II)/Ru(III) complexes. It has long been known that chemical waves in thin layers of the BZ reaction are susceptible to hydrodynamic perturbations that in the presence of a free solution/air interface result from a Marangoni instability.[18] The resulting fluid convection can alter the reaction−diffusion dynamics of the system and even nucleate or destroy spiral waves. To avoid these perturbations, the reaction can be carried in polymer matrices of which agarose, silica, and polyacrylamide gels as well as naphion and polysulfone membranes have been popular choices that withstand the harsh conditions presented by the BZ chemistry.[19−21]

A particularly interesting perturbation of the spiral wave is the pinning of the spiral tip to an unexcitable and/or impermeable heterogeneity.[22,23] This scenario was first considered by Wiener and Rosenblueth in 1941, who investigated spiral wave rotation around a hole using a cellular automaton model.[24] More than 50 years later, Steinbock and Müller demonstrated spiral pinning in experiments with the photosensitive $Ru(bpy)_3$-catalyzed BZ reaction by creating an inhibited pinning site with an argon ion laser.[22] More recently, a theoretical study by Biktashev et al. reported that small heterogeneities of higher excitability can induce orbital motion

Received: June 17, 2014
Revised: July 29, 2014
Published: July 31, 2014

dx.doi.org/10.1021/jp5060292 | J. Phys. Chem. A 2014, 118, 6819−6826

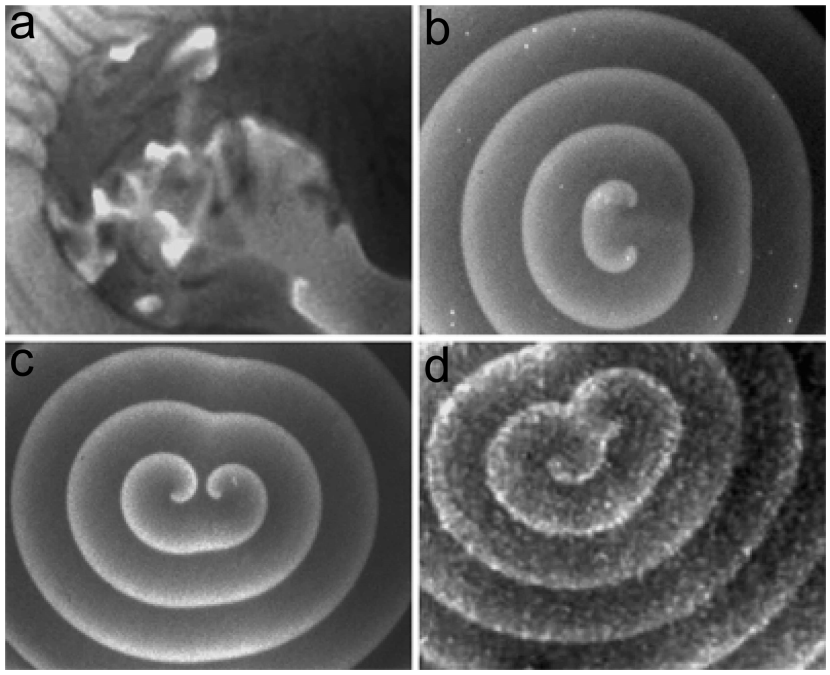

Figure 1. Wave patterns in a thin layer of the BZ solution with xanthan gum concentrations of 0.0 (a), 0.05 (b), 0.4 (c), and 1.0% w/v (d). Bright and dark areas indicate high and low concentrations of the oxidized catalyst (ferriin), respectively. Field of view: 2.5 × 2.1 cm^2.

in which the rotation center of the spiral tip orbit revolves along the boundary of the heterogeneity.[25]

In this Article, we report experiments and simulations that demonstrate the pinning of spiral waves to *moving* heterogeneities. The heterogeneities are disk-like glass objects and modeled as circular no-flux boundaries. For these experiments, we increase the viscosity of the BZ reaction by the addition of two different polysaccharides (xanthan gum[26,27] and agar). Our key finding is that spiral pinning under such conditions is possible, although the slow motion of the heterogeneity creates a Stokes—or creeping—flow[28] in the BZ solution. We suggest that the techniques described in this Article are applicable to three-dimensional BZ systems, thus opening up new possibilities for the study and control of three-dimensional scroll waves.[29]

EXPERIMENTAL METHODS

Stock solutions of sodium bromate (Acros Organics), malonic acid ($CH_2(COOH)_2$; Sigma-Aldrich), sulfuric acid (Ricca Chemical Co.), ferroin ($Fe(phen)_3SO_4$; Sigma-Aldrich), and 0.1% w/v agar solution (Sigma-Aldrich) are prepared with deionized water (18 MΩ cm, Easy-pure UV, Barnstead) and kept at room temperature. For each experiment, the desired amount of xanthan gum (Sigma-Aldrich) and 10.0 mL water are first added into 25.0 mL of 0.1% w/v agar solution. To dissolve the xanthan gum, this mixture is carefully heated and stirred at 600 rpm for 20−30 min. After the solution has cooled to room temperature, 3.75 mL of H_2SO_4 (2.5 M), 3.11 mL of $NaBrO_3$(aq) (1.0 M), 2.40 mL of malonic acid solution (1.0 M), and 0.375 mL of $Fe(phen)_3SO_4$(aq) (5.0 mM) are mixed together. By adding an appropriate amount of deionized water, the total solution volume is adjusted to 50.0 mL, which—disregarding the bromination and oxidation of malonic acid—yields the following initial concentrations: [malonic acid] = 48.0 mM, [H_2SO_4] = 188 mM, [$NaBrO_3$] = 62.2 mM, and [$Fe(phen)_3SO_4$] = 0.0375 mM.

After stirring at 600 rpm for an additional 20 min, 14.8 mL of the reaction solution is transferred into a glass Petri dish (diameter 5.6 cm) to yield a solution layer height of approximately 0.6 cm. We then generate circular (nonrotating) waves by submerging the tip of a silver wire (diameter 1.0 mm) in the solution for a couple of minutes. These waves are locally disrupted by a glass rod and spiral waves occur at both of the open wave ends. A charge-coupled-device camera (COHU 2122-1000) equipped with a dichroic blue filter is used to monitor the evolution of the chemical wave patterns. The video camera is positioned underneath the Petri dish. Image contrast results from the absorption of light by the chemically reduced form of the iron complex. Wave patterns in our experiments can be observed for more than 6 h.

After stable spiral rotation is observed, a glass rod (diameter 1.1 mm) is positioned close to the tip of a spiral wave. In our experiments, the vertical glass rod is essentially submerged across the whole solution layer allowing only for a very small gap to the glass surface of the Petri dish. This gap is necessary to avoid friction-induced velocity variations (or jamming) of the moving glass rod. The motion of the glass rod is generated by a motor-driven linear actuator for which we adapt a commercial syringe pump (New Era Pump Systems, Inc., NE-1600). All experiments are carried out at room temperature.

Our viscosity measurements are performed with a rotational rheometer (Thermo Scientific HAAKE RheoStress 300). The data reported here are obtained at a rotation frequency of 1.0 Hz. This low frequency was chosen because the shear rates in our vortex pinning experiments are very small. Polymer solutions without the BZ reagents are analyzed 1 h after preparation.

EXPERIMENTAL RESULTS

Figure 1 shows representative wave patterns observed in four BZ solutions that differ only in their concentrations of agar and xanthan gum (XG). In the absence of viscosity-increasing

dx.doi.org/10.1021/jp5060292 | J. Phys. Chem. A 2014, 118, 6819−6826

polymers (a), we do not observe stable wave patterns. Reaction−diffusion waves are quickly perturbed by fluid convection that is most likely caused by a Marangoni instability[30] at the free solution−air interface. Similar chemo-hydrodynamic patterns have been reported in ref 18. Addition of only 0.05% w/v agar suppresses such spontaneous fluid motion and we observe isotropic and well ordered chemical wave patterns as exemplified by the spiral wave pair in Figure 1b. We attribute this effect to the polymer-dependent increase in the solution viscosity. This convection-free BZ system serves as the reference point for the addition of XG that allows us to adjust the solution viscosity over a wide range of values. Notice that agar is not suitable for this purpose as higher concentrations of agar (or agarose) tend to compromise the spatial homogeneity of the system and also strongly increase the system opacity.

The usable range of XG concentrations for our BZ system extends from zero to about 1.0% w/v. Figure 1c shows that, if compared to Figure 1b, an addition of 0.05% w/v causes no detectable changes in the observed wave pattern. Even at the high concentration of 1.0% w/v (Figure 1d), the pattern wavelength remains essentially unchanged but we notice a grainy appearance of the BZ system. This feature is caused by a multitude of reaction-induced CO_2 bubbles. At this high polymer concentration, bubble nucleation is greatly enhanced but, due to the system's high viscosity, these bubbles do not rise in the solution.

The rotation period, wavelength, and wave velocity of spiral waves are system-specific values that are fully determined by the reactant concentrations of the BZ system and the system temperature.[31] As in many other BZ studies that employ thermodynamically closed conditions, the wave patterns slowly change during the course of the reaction. Over time this "aging" causes typically slower wave propagation and larger wavelengths. These effects are also found in our study, yielding wavelengths and wave velocities in the ranges of 3.5−5.5 mm and 17−23 μm/s, respectively. In addition, our system shows steadily decreasing rotation periods. As illustrated in Figure S1 of the Supporting Information, the period in the XG-free system decreases from 320 to 215 s during the first 6 h of reaction. Addition of XG shortens rotation periods and also decreases the rate at which the period changes over time. At XG concentrations of 0.8 and 1.0% w/v, this trend results in nearly constant periods of 180 s (Figure S2, Supporting Information). The mechanism behind this effect is unknown but our results indicate that XG is not a chemically inert additive. It seems possible that XG acts as a sink for inhibitory bromide species and/or accelerates the reduction of the oxidized iron catalyst.

Figure 2 characterizes the dynamic (shear) viscosity of XG and XG-BZ solutions. In (a) we report the viscosity of the polymer solution as a function of the XG concentration. These samples contained 0.05% w/v agar but no BZ reagents; however, our measurements show that the influence of the BZ constituents, which are all of a low molecular weight, is very small compared to the polymer. In Figure 2b we evaluate the time evolution of the viscosity of a XG-BZ system at a XG concentration of 0.4% w/v. Our results show that there are no reaction-induced changes in the viscosity. Moreover, the time average of 76 cP is very close to the viscosity expected from the data shown in Figure 2a. Notice that addition of 1.0% w/v XG increases the viscosity from about 7 cP (0.05% w/v agar) to 240

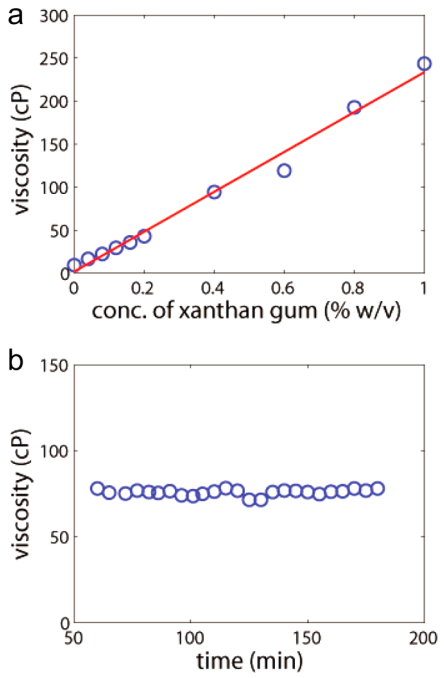

Figure 2. (a) Viscosity of xanthan gum solutions containing 0.05% w/v agar but no BZ reagents. The red, continuous line is the best linear fit of the experimental data (blue circles). (b) Time-resolved measurement of the viscosity of a BZ solution containing 0.4% w/v xanthan gum and 0.05% w/v agar.

cP. All subsequent experiments employ a XG concentration of 0.4% w/v.

The increased viscosity of the XG-BZ system allows us to move a glass rod through the solution layer without causing long-range perturbations of the chemical wave patterns. In addition, we can pin spiral waves to the glass rod and then reposition the spiral tip by a slow translational motion of the rod. A representative example for such an experiment is shown in Figure 3. In this experiment, we follow a pair of counter-rotating spiral waves. In the first snapshot (a), their tips are spaced at a distance of less than one pattern wavelength. The right spiral tip is pinned to a glass rod with a diameter of 1.1 mm. After a few rotation periods, we move the rod in a downward direction (b)−(d). During this process the spiral tip remains attached to the impermeable heterogeneity and follows its motion while continuing its counterclockwise rotation. The velocity of the pinning site is 0.18 mm/min. This value is about 6 times smaller than the average wave speed of 1.06 mm/min. Notice that during the repositioning of the right spiral, the free, left tip remains at its original location. In addition, we do not observe any large-scale deformations of the wave patterns due to fluid flow around the moving glass rod.

Figure 3e is a time−space plot constructed from intensity profiles collected along the trajectory of the glass rod. The moving glass rod creates a wide, diagonal band while the narrow, bright bands correspond to individual wave pulses. The pinned spiral emits waves in the left and rightward directions. In the upper left segment of the plot we also observe wave pulses that emanate from the free spiral wave. These reaction fronts collide with the waves of the pinned spiral to form Λ-shaped cusps in the wake of the moving rod. As expected, these collision points move rightwards but over time they increase their distance to the glass rod. This expansion of the pinned

dx.doi.org/10.1021/jp5060292 | J. Phys. Chem. A 2014, 118, 6819−6826

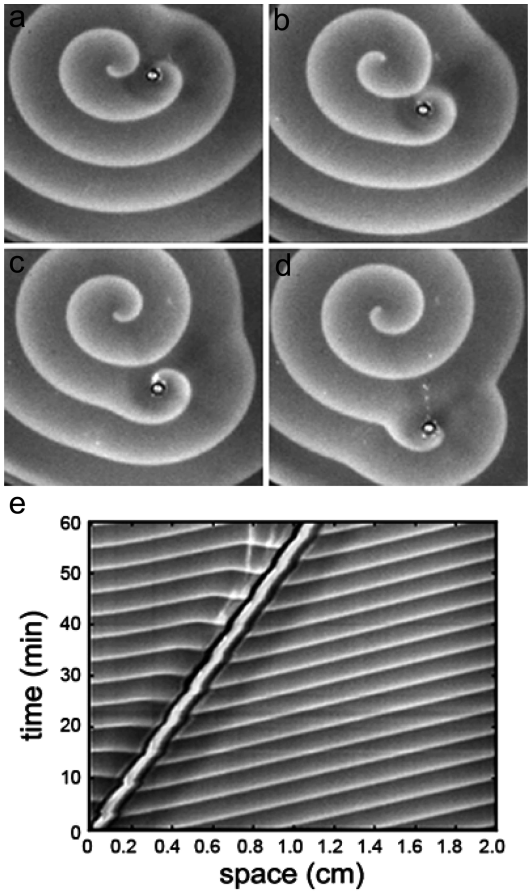

Figure 3. (a)−(d) Image sequence showing the repositioning of a pinned spiral wave in a thin layer of the BZ solution. The viscosity of the system has been increased by addition of 0.05% w/v agar and 0.4% w/v xanthan gum. Time between frames: (a), (b) 1200 s; (b), (c) 1200 s; (c), (d) 1400 s. Field of view: 2.6 × 2.4 cm^2. (e) Time−space plot of the experiment in (a)−(d) constructed along the trajectory of the moving heterogeneity.

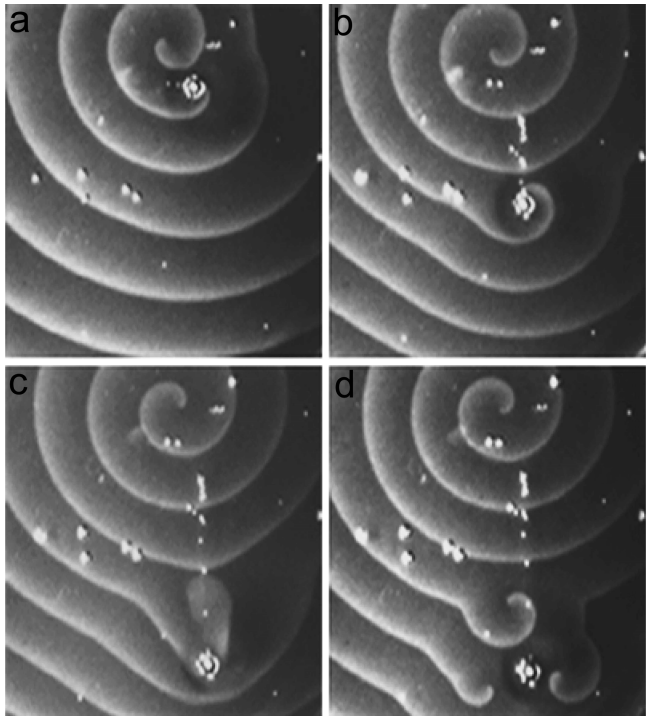

Figure 4. Response of the system to a sudden increase in the velocity of the pinning heterogeneity. The pinned spiral (a) follows the slowly moving glass disk (b) but when the speed is increased from 3 to 12 μm/s, it loses contact (c) and the heterogeneity induces a new spiral wave pair (d). Time between frames: (a), (b) 3548 s; (b), (c) 748 s; (c), (d) 2658 s. Field of view: 2.7 × 3.0 cm^2.

wave field is surprising and might be the result of a pinning-induced increase in rotation frequency.

The experiment in Figure 4 probes the response of the pinned and moving spiral tip to a sudden increase in the speed of the heterogeneity. In (a) and (b), the glass rod is moving at a speed of 0.18 mm/min and the spiral tip follows successfully. Shortly after (b), the speed is increased to 0.72 mm/min. In response, the originally pinned tip loses contact and after a transient period of mild shape deformations (c) and settles into a new stationary position (d). Notice that the shape deformations of the unpinned spiral in (c) include a widened, "washed out" wavefront. In addition, we find that the fast moving heterogeneity breaks the wavefront ahead of the tip and nucleates a new pair of spiral waves (see lower edge of Figure 4d). From several, systematic experiments we estimate the maximal pinning velocity as 0.36 mm/min.

MODEL AND COMPUTATIONAL METHODS

To obtain further insights into the pinning of spiral waves to moving heterogeneities, we perform numerical simulations based on the Barkley model,[12,32] which is frequently used to simulate waves in excitable media. This reaction−diffusion model includes two variables, u and v, performing as the activator and the control species in the system. To accord with the experiments, we extend the Barkley model by adding advection terms to both the u and v variables. The advection terms describe the fluid dynamics of the excitable media when the heterogeneity is moving. The complete model equations are

$$\frac{\partial u}{\partial t} = D_u \vec{\nabla}^2 u + \varepsilon^{-1} u(1-u)\left(u - \frac{v+b}{a}\right) - \vec{c}\vec{\nabla}u \quad (1)$$

$$\frac{\partial v}{\partial t} = D_v \vec{\nabla}^2 v + (u - v) - \vec{c}\vec{\nabla}v \quad (2)$$

In this model, the parameters ε, a, and b are kept constant at 0.02, 0.9, and 0.08, respectively. In our simulations, the two diffusion coefficients always obey $D_u = D_v$ and are varied between 0.1 and 10. For this set of parameters, the trajectory of the unperturbed spiral tip is a simple circle. The two-dimensional vector field $\vec{c}$ in the advection terms consists of the components c_x and c_y that describe the velocity of the fluid in the x and y directions, respectively. To obtain the proper expression for this flow field, we follow a well-established method[28] and consider the streamline function in polar coordinates (r, θ):

$$\psi = -\frac{V_d R^2}{r}\sin\theta \quad (3)$$

In three dimensions, this streamline function describes the Stokes flow generated when a cylinder of radius R slowly moves through an otherwise static fluid with a velocity V_d. We transform eq 3 to Cartesian coordinates (x, y)

$$\psi = -\frac{V_d R^2}{r^2} y \quad (4)$$

dx.doi.org/10.1021/jp5060292 | J. Phys. Chem. A 2014, 118, 6819−6826

and then derive c_x and c_y from $c_x = -\partial\psi/\partial y$ and $c_y = \partial\psi/\partial x$

$$c_x = \frac{V_d R^2}{r^2} - \frac{2V_d R^2}{r^4} y^2 \quad (5)$$

$$c_y = \frac{2V_d R^2}{r^4} xy \quad (6)$$

Equations 1 and 2 are integrated by the explicit forward Euler scheme with a typical space step of 0.25 and a time step of 6.25×10^{-3}. In Figure 6 the grid spacing is 0.1 in (a), (b) and 0.6 in (c), (d) and the time step is 1.0×10^{-3} in (a), (b) and 3.6×10^{-3} in (c), (d). In most simulations, the lattice measures 300×300 spaces units and is represented by 1200×1200 grid points. A five-point stencil is used to evaluate the Laplacian. The initial state of the system contains a spiral wave pair, one of which is pinned to a circular heterogeneity. The spiral wave pair is generated by creating an excited stripe ($u = 0.8$) next to an inhibitor stripe ($v = 0.5$), located at the center of an otherwise excitable space ($u = 0$, $v = 0$). The two ends of the excited stripe bend toward the v-bar and nucleate the desired spiral wave pair. To ensure transient-free pinning, we wait for ten rotation cycles prior to moving the heterogeneity. In all figures, the heterogeneity moves in the downward direction (Figure 5).

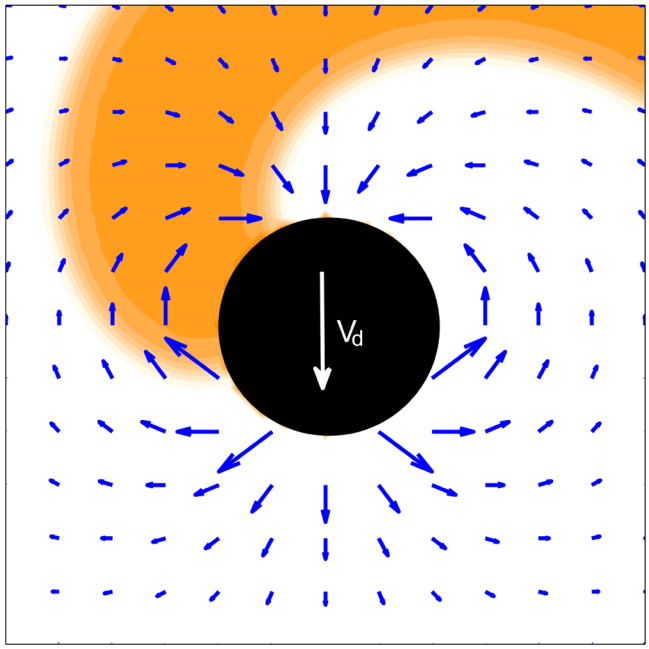

Figure 5. Simulation of a counterclockwise rotating spiral wave (orange band representing high u values) in a dimensionless reaction–diffusion-flow model. The spiral tip is pinned to a circular heterogeneity (black disk). This disk has a no-flux boundary and moves at a speed of V_d. The Stokes flow generated by this motion is shown as the blue vector field for which the vector length is proportional to the local velocity of the fluid. For the parameters $V_d = 0.6$, $R = 2.5$, and $D_u = D_v = 1.0$ used in this example, the flow occurs mainly near the spiral center.

The lattice has periodic boundaries along the top and bottom edges and Neumann (no-flux) boundaries along the left and right edges. Notice that the system must be sufficiently large to ensure that at these boundaries the flow field defined by eqs 5 and 6 has decayed to very small values. We implement Neumann boundaries for the moving disk using the phase-field method reported in ref 33. For this, we define a field ϕ, which is equal to 0 inside of the moving disk and equal to 1 outside of it. The interface is smoothed by applying the function

$$\phi(r) = \frac{1}{2} + \frac{1}{2}\tanh((r - R)/\xi) \quad (7)$$

where R is the radius of the disk and r measures the distance to the center of the disk. The parameter ξ determines the width of the interface and is kept constant at 0.25 for all our simulations. The original variables u and v in the eqs 1 and 2 are substituted by ϕu and ϕv, yielding

$$\frac{\partial(\phi u)}{\partial t} = \vec{\nabla}\cdot(D_u \phi \vec{\nabla} u) + \phi\varepsilon^{-1}u(1-u)\left(u - \frac{v+b}{a}\right) - \phi\vec{c}\vec{\nabla}u \quad (8)$$

$$\frac{\partial(\phi v)}{\partial t} = \vec{\nabla}\cdot(D_v \phi \vec{\nabla} v) + \phi(u - v) - \phi\vec{c}\vec{\nabla}v \quad (9)$$

COMPUTATIONAL RESULTS

The main features of our model are illustrated by the simulation result in Figure 5. The spiral tip is tightly attached to the Neumann boundary of the disk, which is a realistic representation of the experimental situation. The blue arrows denote the flow field generated by the downward moving disk. Notice that in this example, the fluid velocity decreases to nearly zero over a distance of less than one wavelength of the spiral. This relation, however, can be changed by varying the flow-field defining parameters (R and V_d) and/or the wavelength-selecting parameters of the reaction–diffusion core of our model. Among the latter parameters, the diffusion coefficients ($D_u = D_v$) are a convenient choice because, in the absence of fluid motion, they affect the pattern wavelength λ according to $\lambda \propto D_u^{1/2}$. The latter approach is used in the following to evaluate the relation between the flow-controlled and the reaction–diffusion-dependent length scales.

Figure 6 shows two different simulations of a spiral wave pair in a large domain. Panels a and b represent the entire system area, whereas panels c and d show only a smaller section and omit one of the two rotors. In each case, one of the spirals is pinned to a (downward) moving disk. The simulations differ only in their diffusion coefficients yielding a short vortex wavelength for $D_u = D_v = 0.1$ in (a,b) and a long wavelength for $D_u = D_v = 10$ in (c,d). Also the time elapsed between the frames (a), (b) and (c), (d) is identical.

The dynamics illustrated by the snapshots in Figure 6c,d are similar to the behavior of the experimental system. The spiral is firmly pinned to the disk and rotates around this heterogeneity while being transported in the downward direction. We note that this scenario is similar to the response of spirals pinned to moving laser spots in photosensitive, convection-free BZ systems.[22] The wave dynamics in Figure 6a,b, however, are markedly different and clearly reflect the presence of fluid flow. While the spiral tip is also pinned to the disk, it fails to rotate around the heterogeneity and rather forms a trailing, straight wave segment. Moreover, the downmost wavefront is strongly deformed ahead of the moving disk. Clearly, this wave is faster than the unperturbed fronts as it is being pushed forward by the disk's flow field. We reemphasize that the disk radius and the disk speed are identical in these two simulations, thus generating identical flow fields around the moving heterogeneities.

dx.doi.org/10.1021/jp5060292 | J. Phys. Chem. A 2014, 118, 6819–6826

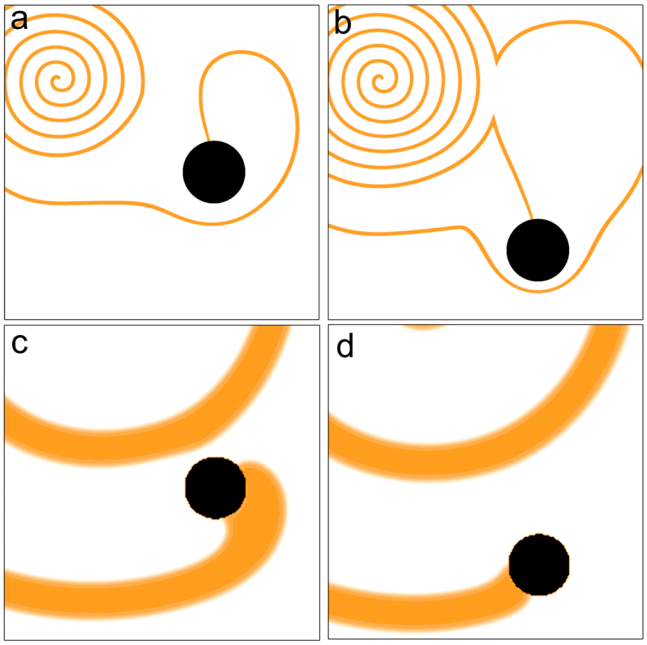

Figure 6. Two simulations illustrating the influence of the diffusion coefficient on the pinning and repositioning process. (a), (b) Two snapshots of a simulation at $D_u = D_v = 0.1$. Here the tip is pinned to the heterogeneity (black disk) but does not rotate. (c), (d) Two snapshots of a simulation at $D_u = D_v = 10.0$, for which the impact of the flow field is small. All other parameters are identical for the simulations in (a), (b) and (c), (d) including $V_d = 2.4$ and $R = 12$. The time elapsed between the frames (a), (b) and (c), (d) is 12.42.

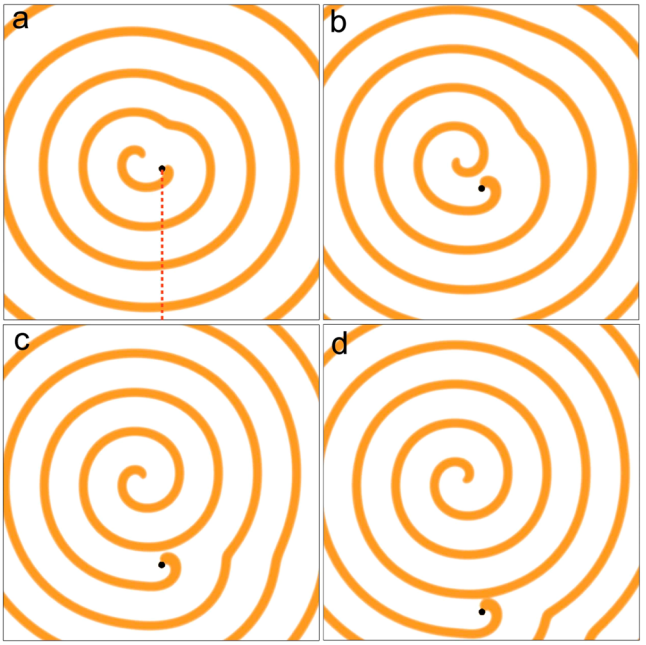

Figure 7. (a)−(d) Sequence of snapshots of a spiral wave pinned to a moving heterogeneity (small black disk). The red dotted line in (a) is the trajectory of the downward moving disk. Only a quarter of the simulation space is shown. Model parameters: $V_d = 0.6$, $R = 2.5$, and $D_u = D_v = 1.0$.

We suggest that certain aspects of the scenarios shown in Figure 6 can be evaluated in terms of a Péclet number *Pe* that compares the rate of advective transport to that of diffusion

$$Pe = RV_d/D_u \tag{10}$$

using the disk radius *R* as the characteristic length. *Pe* is related to the Reynolds number *Re* and the Schmidt number *Sc* by $Pe = Sc \times Re$ where *Sc* is the ratio of the kinematic viscosity to the diffusion coefficient. For the simulations shown in Figure 6, the dimensionless number *Pe* equals 288 in (a), (b) and 2.88 in (c), (d). Accordingly, these simulations are examples for strong (a), (b) and (by comparison) weak Stokes flow (c), (d).

We also evaluate whether our simulations can reproduce the repositioning of a spiral over larger distances. With this goal in mind, we first determine a lower limit for the experimental Péclet number. The relevant parameters of the experiment in Figure 3 are $R = 0.055$ cm and $V_d = 3 \times 10^{-4}$ cm/s. If we further consider the diffusion coefficient of the autocatalytic species ($HBrO_2$) in water ($D = 2 \times 10^{-5}$ cm^2/s), we obtain $Pe = 0.83$. Any polymer-induced decrease in *D* would increase *Pe* but such changes cannot be large because the spiral wavelength does not change significantly with the XG concentration (Figure 1).

The computational results in Figure 7 are obtained for conditions that correspond to $Pe = 1.5$, which should be a sufficiently close representation of the experiment in Figure 3. In addition, we adjusted V_d to match the experimental disk-to-wave speed ratio that we measured as 0.19. The simulation involves a spiral wave pair for which one tip is pinned to an impermeable, disk-shaped object. This starting condition is shown in Figure 7a where the pinning heterogeneity is plotted as a black disk. After several rotations of the pinned vortex, we steadily move the heterogeneity along the red dotted line in the downward direction. The subsequent frames (Figure 7b−d) show that the spiral tip remains pinned during this process. In addition, we observe no position change for the free, clockwise rotating spiral. These observations are in good agreement with the experiment. We can further conclude that in both the experiment (Figure 3) and the simulation (Figure 7), the impact of the Stokes flow on the reaction−diffusion vortex is small and tightly localized around the disk. This conclusion is further supported by an evaluation of eqs 5 and 6 because the corresponding equation $c(r) = V_dR^2/r^2$ predicts a rapid decay of the fluid flow. For instance, in the experiment shown in Figure 3, we use $V_d = 3 \times 10^{-3}$ mm/s and $R = 0.55$ mm, which implies that the fluid speed decreases down to 10% over a distance of 1.74 mm as measured from the disk center and 1.19 mm as measured from the edge of the heterogeneity. The latter value is approximately one-quarter of the wavelength of the free spiral (4.7 mm).

Figure 8 shows a time−space plot for the simulation in Figure 7. The diagram is constructed from a sequence of *u*-profiles obtained along the trajectory of the moving disk. The disk motion generates the wide, blue stripe whereas the thinner, black bands are generated by individual wave pulses. Overall, the dynamics summarized in Figure 8 are in excellent, qualitative agreement with the experimental data in Figure 3e.

Lastly, we note that the pinning-mediated repositioning of spiral waves is only possible up to a maximal disk speed. We did not systematically investigate this limit yet because in our model it depends on six different parameters and possibly on factors such as neighboring wave patterns and phase relations. However, results similar to the one in Figure 6a,b indicate that the fluid flow around the moving disk can *stabilize* the pinned wave pattern, thus allowing the repositioning of the tip at speeds that are not possible without Stokes flow. This perhaps counterintuitive result can be seen in Figure 6a,b where the

dx.doi.org/10.1021/jp5060292 | J. Phys. Chem. A 2014, 118, 6819−6826

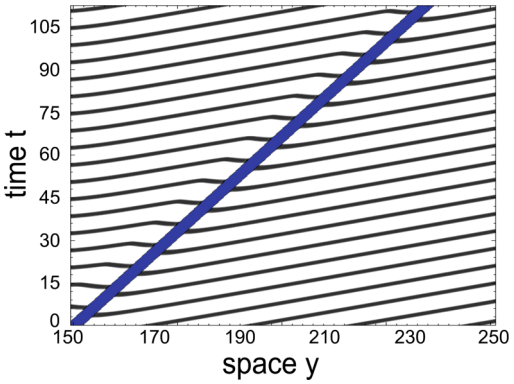

Figure 8. Time−space plot obtained from the simulation shown in Figure 7. The plot shows the wave dynamics along the trajectory of the moving heterogeneity. This disk motion generates the wide, blue stripe where as all black bands correspond to high *u* values.

ratio of disk to wave speed is larger than 1. In the absence of Stokes flow, such a fast heterogeneity would rapidly lose the spiral tip.

CONCLUSIONS

This study establishes xanthan gum as a convenient choice for creating highly viscous BZ systems. The polymer is commercially available and has a sufficiently small impact on the aggressive BZ chemistry. In this respect it adds a valuable alternative to the use of polyacrylamide that up to now has been the exclusive choice for the study convection-free, liquid BZ systems.[34] We reemphasize that viscous BZ media allow for a wide range of experimental studies that cannot be carried out in gel or membrane-based systems. One important example is the study of self-motion in BZ systems;[35] others include the controlled creation of three-dimensional scroll waves and their manipulation by physical obstacles and reactive solids such as inhibitory iron and activating silver wires.[9,36] In this context, it is important that the flow field around the moving disk can be much smaller than the spiral pitch, thus causing only weak perturbations to the wave pattern. This scenario seems ideally suited for future investigations of scroll waves pinned[17,29] to *moving* heterogeneities.

In addition our approach contributes to the expanding field of chemo-hydrodynamics.[37−39] Specifically, our results open up new possibilities for the study of chemical self-organization under the influence of fluid motion that is (i) not affected by the concentration pattern and (ii) well characterized and simple (at least by comparison to Marangoni[18] and other complex flows). So far, this type of reaction−diffusion-flow systems had been investigated primarily in the context of linear shear flow and for flow-driven instabilities in laminar pipe flow.[40,41] In the spirit of our work, we suggest that future studies could evaluate specifically the impact of creeping flow generated by rotating disks which we expect to create chirality-dependent perturbations on spiral waves. Additional studies are also needed for a satisfactory description of the effects of translating heterogeneities. Among the unstudied phenomena, we emphasize the flow-induced disruption and subsequent nucleation of spiral waves which clearly deserves quantitative investigations.

ASSOCIATED CONTENT

Supporting Information

Figures showing the time dependence of the rotation period for various concentrations of xanthan gum and additional data on flow-induced wave deformations. Movies of the experiment in Figure 3 and the simulation in Figure 6a,b. This material is available free of charge via the Internet at http://pubs.acs.org

AUTHOR INFORMATION

Corresponding Author

*O. Steinbock. E-mail: steinbck@chem.fsu.edu.

Notes

The authors declare no competing financial interest.

ACKNOWLEDGMENTS

This work is supported by the National Science Foundation under Grant No. 1213259.

REFERENCES

(1) Epstein, I. R.; Pojman, J. A. *An Introduction to Nonlinear Chemical Dynamics*; Oxford University Press: New York, 1998.
(2) Epstein, I. R.; Vanag, V. K.; Balazs, A. C.; Kuksenok, O.; Dayal, P.; Bhattacharya, A. Chemical Oscillators in Structured Media. *Acc. Chem. Res.* **2012**, *45*, 2160−2168.
(3) Tinsley, M. R.; Taylor, A. F.; Huang, Z.; Showalter, K. Complex Organizing Centers in Groups of Oscillatory Particles. *Phys. Chem. Chem. Phys.* **2011**, *13*, 17802−17808.
(4) Sawai, S.; Thomason, P. A.; Cox, E. C. An Autoregulatory Circuit for Long-Range Self-Organization in Dictyostelium Cell Populations. *Nature* **2005**, *433*, 323−326.
(5) Cherry, E. M.; Denton, F. H.; Gilmour, R. F., Jr. Mechanisms of Ventricular Arrhythmias: A Dynamical Systems-Based Perspective. *Am. J. Physiol Heart Circ. Physiol.* **2013**, *302*, H2451−H2463.
(6) Pervolaraki, E.; Holden, A. V. Spatiotemporal Patterning of Uterine Excitation Patterns in Human Labour. *Biosystems* **2013**, *112*, 63−72.
(7) Sadeghi, P.; Dunphy, K.; Punckt, C.; Rotermund, H. H. Inversion of Pattern Anisotropy During CO Oxidation on Pt(110) Correlated with Appearance of Subsurface Oxygen. *J. Phys. Chem. C* **2012**, *116*, 4686−4691.
(8) Agladze, K.; Steinbock, O. Waves and Vortices of Rust on the Surface of Corroding Steel. *J. Phys. Chem. A* **2000**, *104*, 9816−9819.
(9) Jiménez, Z. A.; Marts, B.; Steinbock, O. Pinned Scroll Rings in an Excitable System. *Phys. Rev. Lett.* **2009**, *102* (244101), 1−4.
(10) Riaz, S. S.; Ray, D. S. Spiral Pattern in Chlorite-Iodide-Malonic Acid Reaction: A Theoretical and Numerical Study. *J. Chem. Phys.* **2005**, *123* (174506), 1−5.
(11) Winfree, A. T. Spiral Waves of Chemical Activity. *Science* **1972**, *175*, 634−636.
(12) Barkley, D. Euclidian Symmetry and the Dynamics of Rotating Spiral Waves. *Phys. Rev. Lett.* **1994**, *72*, 164−167.
(13) Brandtstädter, H.; Braune, M.; Schebesch, I.; Engel, H. Experimental Study of the Dynamics of Spiral Pairs in Light-Sensitive Belousov-Zhabotinskii Media Using an Open-Gel Reactor. *Chem. Phys. Lett.* **2000**, *323*, 145−154.
(14) Biktasheva, I. V.; Barkley, D.; Biktashev, V. N.; Bordyugov, G. V.; Foulkes, A. J. Computation of the Response Functions of Spiral Waves in Active Media. *Phys. Rev. E* **2009**, *79* (056702), 1−10.
(15) Steinbock, O.; Zykov, V. S.; Müller, S. C. Synchronization of Spiral Waves in Active Media by Periodic Modulation of Excitability. *Nature* **1993**, *366*, 322−324.
(16) Vinson, M.; Mironov, S.; Mulvey, S.; Pertsov, A. Control of Spatial Orientation and Lifetime of Scroll Rings in Excitable Media. *Nature* **1997**, *386*, 477−480.

(17) Jiménez, Z. A.; Steinbock, O. Stationary Vortex Loops Induced by Filament Interaction and Local Pinning in a Chemical Reaction-Diffusion System. *Phys. Rev. Lett.* **2012**, *109* (098301), 1−4.
(18) Sakurai, T.; Miike, H.; Okada, K.; Müller, S. C. Spiral Flow Wave in a Reaction-Diffusion-Covection System. *J. Phys. Soc. Jpn.* **2003**, *72*, 2177−2180.
(19) Yamaguchi, T.; Kuhnert, L.; Nagy-Ungvarai, Z.; Müller, S. C.; Hess, B. Gel Systems for the Belosuov-Zhabotinskii Reaction. *J. Phys. Chem.* **1991**, *95*, 5831−5837.
(20) Steinbock, O.; Kettunen, P.; Showalter, K. Anisotropy and Spiral Organizing Centers in Patterned Excitable Media. *Science* **1995**, *267*, 868−871.
(21) Nakata, S.; Yoshii, M.; Suzuki, S.; Yoshida, R. *Langmuir* **2014**, *30*, 517−521.
(22) Steinbock, O.; Müller, S. C. Chemical Spiral Rotation is Controlled by Light-Induced Artificial Cores. *Physica A* **1992**, *188*, 61−67.
(23) Tanaka, M.; Isomura, A.; Horning, M.; Kitahata, H.; Agladze, K.; Yoshikawa, K. Unpinning of a Spiral Wave Anchored Around a Circular Obstacle by an External Wave Train: Common Aspects of a Chemical Reaction and Cardiomyocyte Tissue. *Chaos* **2009**, *19* (043114), 1−5.
(24) Wiener, N.; Rosenblueth, A. The Mathematical Formulation of the Problem of Conduction of Impulses in a Network of Connected Excitable Elements, Specifically in Cardiac Muscle. *Arch. Inst. Cardiol. Mex.* **1946**, *16*, 205−265.
(25) Biktashev, V. N.; Barkley, D.; Biktasheva, I. V. Orbital Motion of Spiral Waves in Excitable Media. *Phys. Rev. Lett.* **2010**, *104* (058302), 1−4.
(26) Gracía-Ochoa, F.; Santos, V. E.; Casas, J. A.; Gómez, E. Xanthan Gum: Production, Recovery, and Properties. *Biotechnol. Adv.* **2000**, *18*, 549−579.
(27) Whitcomb, P. J.; Macosko, C. W. Rheology of Xanthan Gum. *J. Rheol.* **1978**, *22*, 493−505.
(28) Lamb, H. *Hydrodynamics*, 6th ed.; Dover: New York, pp 76−78.
(29) Jiménez, Z. A.; Steinbock, O. Scroll Wave Filaments Self-Wrap Around Unexcitable Heterogeneities. *Phys. Rev. E* **2012**, *86* (036205), 1−9.
(30) Velarde, M. G. Drops, Liquid Layers and the Marangoni Effect. *Philos. Trans. R. Soc. A* **1998**, *356*, 829−844.
(31) Belmonte, A. L.; Quyang, Q.; Flesselles, J.-M. Experimental Survey of Spiral Dynamics in the Belousov-Zhabotinsky Reaction. *J. Phys. II Fr.* **1997**, *7*, 1425−1468.
(32) Barkley, D. A Model for Fast Computer Simulation of Waves in Excitable Media. *Physica D* **1991**, *49*, 61−70.
(33) Fenton, F. H.; Cherry, E. M.; Karma, A.; Rappel, W. J. Modeling Wave Propagation in Realistic Heart Geometries Using the Phase-Field Method. *Chaos* **2005**, *15* (013502), 1−11.
(34) Bánsági, T., Jr.; Steinbock, O. Negative Filament Tension of Scroll Rings in an Excitable System. *Phys. Rev. E* **2007**, *76* (045202), 1−4.
(35) Szymanski, J.; Gorecki, J.; Hauser, M. J. B. Chemo-Mechanical Coupling in Reactive Droplets. *J. Phys. Chem. C* **2013**, *117*, 13080−13086.
(36) Kupitz, D.; Hauser, M. J. B. Interaction of a Pair of Scroll Waves. *J. Phys. Chem. A* **2013**, *117*, 12711−12718.
(37) Schwartz, M. E.; Solomon, T. H. Chemical Reaction Fronts in Ordered and Disordered Cellular Flows with Opposing Winds. *Phys. Rev. Lett.* **2008**, *100* (028302), 1−4.
(38) Pópity-Tóth, E.; Horváth, D.; Tóth, A. Horizontally Propagating Three-Dimensional Chemo-Hydrodynamic Patterns in the Chlorite-Tetrathionate Reaction. *Chaos* **2012**, *22* (037105), 1−6.
(39) Escala, D. M.; Budroni, M. A.; Carballido-Landeira, J.; De Wit, A.; Muñuzuri, A. P. Self-Organized Traveling Chemo-Hydrodynamic Fingers Triggered by a Chemical Oscillator. *J. Phys. Chem. Lett.* **2014**, *3*, 413−418.
(40) Tóth, R.; Papp, A.; Gaspar, V.; Merkin, J. H.; Scott, S. K.; Taylor, A. F. Flow-Driven Instabilities in the Belousov-Zhabotinsky Reaction: Modelling and Experiments. *Phys. Chem. Chem. Phys.* **2001**, *3*, 957−964.
(41) Biktashev, V. N.; Biktasheva, I. V.; Holden, A. V.; Tsyganov, M. A.; Brindley, J.; Hill, N. A. Spatiotemporal Irregularity in an Excitable Medium with Shear Flow. *Phys. Rev. E* **1999**, *60*, 1897−1900.